Available online at www.sciencedirect.com
ScienceDirect
Cement and Concrete Research 37 (2007) 823–833
Cement and Concrete Research

Synthesis of cement based $CaO–Al_2O_3–SiO_2–H_2O$ (CASH) hydroceramics at 200 and 250 °C: Ex-situ and in-situ diffraction

Nicola Meller [a,*], Christopher Hall [a], Konstantinos Kyritsis [a], Gaetan Giriat [b]

[a] *Centre for Science at Extreme Conditions and School of Engineering & Electronics, The University of Edinburgh, The King's Buildings, Edinburgh EH9 3JZ, UK*
[b] *Centre for Science at Extreme Conditions and School of Chemistry, The University of Edinburgh, The King's Buildings, Edinburgh EH9 3JZ, UK*

Received 10 November 2006; accepted 7 March 2007

Abstract

Hydroceramic compositions in the $CaO–Al_2O_3–SiO_2–H_2O$ (CASH) system have potential as geothermal well sealants as well as autoclaved construction materials. We report new data on phase compositions and reaction rates in hydrothermal syntheses at 200 °C and 250 °C using a commercial API Class G oilwell cement alone, and at 200 °C with additions of silica flour and of corundum (alumina). Curing times were in the range 1–240 h. We use both ex-situ laboratory X-ray diffraction and in-situ synchrotron energy-dispersive X-ray diffraction to track rates of reaction. When cement only is hydrated, jaffeite, α-C_2SH and portlandite are formed. When silica flour is added a precursory gel forms prior to the crystalline calcium silicate hydrate phases xonotlite and gyrolite. Both XRD and EDD data suggest that the addition of silica flour retards the hydration of the cement at early times (<24 h). In alumina-containing systems the rate of consumption of clinker phases is the same as in cement only systems. Jaffeite and α-C_2SH occur as intermediates but the major end product is a siliceous katoite-type hydrogarnet. Quantitative phase analysis using Rietveld refinement of ex-situ diffraction data gives results which are mostly consistent with stoichiometric constraints in all three systems examined here.

Keywords: Hydration; Kinetics; X-ray diffraction; Oil well cement; Hydroceramics

1. Introduction

Special cement formulations are used as sealants for both oilfield and geothermal wells when the temperature exceeds about 110 °C. Above this temperature the predominant phase formed in the hydration of an oilwell cement, α-dicalcium silicate hydrate α-C_2SH [$Ca_2SiO_3(OH)_2$], forms bulk materials which are too weak and permeable to seal the well [1,2] (note that common cement nomenclature will be used throughout: $C=CaO$, $S=SiO_2$, $A=Al_2O_3$, $F=Fe_2O_3$, $H=H_2O$, $\bar{S}=SO_3$). Upon initial hydration cement first forms a C–S–H gel which on heating converts to crystalline α-C_2SH. This crystallisation causes a reduction in solid volume and is accompanied by an increase in permeability and the reduction in compressive strength known as strength retrogression. Therefore silica is commonly added to cement (approximately 0.35 by wt of cement BWOC) to reduce the C/S ratio to approximately 1.0. This prevents the formation of α-C_2SH and instead a sequence of other calcium silicate hydrates (Fig. 1) form over a range of temperatures [3]. These hydrates produce bulk materials with greater strength and lower permeability. While such cement+silica formulations are normally acceptable for oil wells they are not always durable in the hostile chemical environments encountered in geothermal wells, and formation damage or sealant deterioration or both can occur.

Barlet-Gouédard *et al.* [4–6] and Meller *et al.* [7,8] have recently designed hydroceramics based on the $CaO–Al_2O_3–SiO_2–H_2O$ (CASH) system at 200 and 300 °C. A hydroceramic is defined here as any ceramic composition containing chemically combined water as H_2O or OH or both. While the context of this paper is oil and geothermal well technology, hydroceramics may have wider application as bulk materials for construction. Without knowing how the phase assemblages evolve during curing we cannot be confident that the predicted assemblages will be reached in certain chemical environments.

* Corresponding author.
E-mail address: Nicola.Meller@ed.ac.uk (N. Meller).

0008-8846/$ - see front matter © 2007 Elsevier Ltd. All rights reserved.
doi:10.1016/j.cemconres.2007.03.006

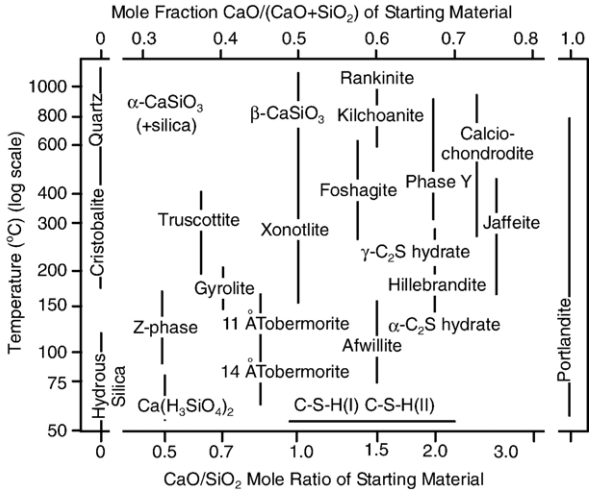

Fig. 1. $CaO–SiO_2–H_2O$ phases from 50 to 1000 °C. After Taylor 1964 [3], with modifications.

If the expected final assemblage is not reached the integrity of the well could be compromised by an inferior sealant. Hence our main aim here is to investigate the kinetics of hydration in pastes and to detect intermediate phases which may exist during curing.

Laboratory and synchrotron X-ray diffraction (XRD) provide ideal tools for such a study. We use ex-situ laboratory XRD to look at the effects of different curing times on hydroceramics formed at 200 °C and to assess the likelihood that intermediate phases exist as major components. Once this is established samples are run using in-situ synchrotron energy dispersive X-ray diffraction EDD to see how the early (<12 h) hydrothermal reactions proceed from different starting compositions and at different curing temperatures. Synchrotron EDD has the advantage over laboratory diffraction that samples are analysed in-situ (hence removing cooling artefacts), and curing times are more precisely known. In addition the X-ray beam penetrates several mm through a bulk sample so that Bragg scattering comes from relatively large volumes, and sample surface and orientation artefacts are largely eliminated.

2. Ex-situ experiments

2.1. Experimental details of ex-situ experiments

Dyckerhoff oilwell cement (API Class G) was used as the basis of the hydroceramics investigated. This commercial cement is widely used and has a consistent composition. The oxide analysis of the cement and the calculated mineralogical composition are summarized in Table 1. The mineralogy from a modified Bogue calculation [9] developed for oil well cements is in rather good agreement with that estimated by Rietveld whole-pattern fitting (mean of ten independent measurements) using Bruker Topas software. The modified Bogue analysis provides estimates of the elemental composition of each of the clinker phases, from which we derive the empirical formula $C_{2.82}S$ to represent the silicate phases of the cement. Silica was added in the form of silica flour HPF6, supplied by Sibelco and composed of 98% silica as quartz SiO_2 with trace impurities and a mean grain size of 53 μm. It is a low cost additive widely used in the cementing of higher temperature wells [2]. Reagent grade α-alumina (corundum Al_2O_3) with a mean grain size of 0.3 μm, supplied by Sigma Aldrich [product code 34271-8], was used as the source of Al_2O_3.

For ex-situ samples a total of 10 g of the starting compounds in the appropriate proportions (Table 2) was mixed with 4 g of water (0.4 by wt of solids BWOS). The sample compositions were chosen to explore the effects of adding silica and alumina separately (but not in combination) to the cement. Each sample paste was mixed by hand and loaded into a polyetheretherketone PEEK polymer cup approximately 3 cm diameter by 1 cm high. Six of these cups were then stacked in a 125 mL capacity stainless steel pressure vessel (type 4750 Parr Instruments), rated at 200 bar at the maximum working temperature of 350 °C. Small notches in the rims of the PEEK cups prevent steam building up between samples and ensure a uniform water-saturated atmosphere throughout. Once sealed, the Parr cell was placed in an oven at 200 °C and left to cure for 1, 2, 24, 48, 120 or 240 h. After curing the Parr Cell was removed from the oven and chilled rapidly in cold water to prevent further reaction. Samples were then left to dry in air before they were removed from the PEEK cups and milled to fine powders for XRD analysis.

A Bruker-AXS D8-series 2 X-ray powder diffractometer, running at 40 kV and 40 mA, was employed for ex-situ analysis. Incident CuK_α radiation was used with a Ge monochromator and passed through a 2 mm monochromator exit slit and 0.2° divergence slit. A Braun position sensitive detector was used to collect data. Diffraction patterns were collected over an angular

Table 1
Chemical and mineralogical composition of Dyckerhoff Class G cement determined by X-ray fluorescence, LECO sulphur analysis and X-ray diffraction

Oxides	Wt.%
Na_2O	0.17
MgO	0.76
Al_2O_3	3.62
SiO_2	22.55
K_2O	0.66
CaO	65.61
TiO_2	0.17
Mn_3O_4	0.14
Fe_2O_3	4.53
SO_3	1.82
Loss on ignition at 1000 °C	1.18
Free Lime	0.40
Insoluble residue	Not determined

%Phases	By modified Bogue method	By Rietveld refinement
Alite C_3S	62	60
Belite C_2S	21	22
Aluminoferrite $C_4(A,F)$	13 (A/F = 0.72)	16
Gypsum CSH_2	3	3

Wt.% phase compositions are calculated from oxide analysis according to the modified Bogue method for oilwell cements [9] and estimated by semi-quantitative Rietveld refinement.

Table 2
Summary of experimental details for ex- and in-situ samples

Sample	Cement	Cement+silica flour (0.67 BWOC)	Cement+alumina (0.67 BWOC)	Cement
Time run ex-situ (h)	1, 2, 24, 48, 120, 240	1, 2, 24, 48, 120	1, 2, 24, 48, 120	–
Time run in-situ (h)	10.5	10.5	10.5	10.5
% Dyckerhoff cement	100	60	60	100
% silica flour	0	40	0	0
% alumina	0	0	40	0
Temperature	200	200	200	250

range of 5 to 70° 2 θ for approximately 30 min total time using a step size of 0.014° 2 θ and a count time of 0.3 s per step.

2.2. Dyckerhoff cement at 200 °C

Although the use of cement alone, without silica addition, is generally avoided in high temperature wells because of the high permeability and low compressive strength of the hydrated bulk material [10], we have used it as a starting point to understand the CASH system. Time-resolved XRD has not been used previously to follow the synthesis of CASH hydroceramics. In order to understand why the sealants exhibit high permeability and low strength it is necessary (if not sufficient) to understand which phases are present and how they change during curing, since the mineralogy strongly influences morphology and hence microstructure.

The cement was hydrated for 1, 2, 24, 48, 120 and 240 h. The anhydrous cement contains alite (impure C_3S), belite (impure C_2S), ferrite (impure C_4(A,F), brownmillerite) and gypsum ($C\overline{S}H_2$). Gypsum cannot be detected after 1 h (Fig. 2) but portlandite CH is visible after that time. Jaffeite $C_6S_2H_3$ and α-C_2SH appear as primary hydration products after 2 h. After 2 h the anhydrous calcium silicates are largely consumed and no further mineralogical changes are observed. The amounts of product phases were estimated quantitatively from the XRD pattern by Rietveld full profile analysis, again using Bruker TOPAS software. This has been used previously to estimate the percentage of phases present during hydration at ambient temperature [11] but not for analysis of those cured at elevated temperatures. Structural data for individual phases were obtained from the Inorganic Crystal Structure Database (ICSD) accessed via the EPSRC's Chemical Database Service at Daresbury [12].

We can write a formal and simplified reaction for the main hydration products:

$$C_{2.82}S[\text{cement}] + h\text{H} \rightarrow jC_6S_2H_3 + cC_2SH + pCH \quad (1)$$

with the stoichiometric relations:

$$c = 1-2j \quad (2)$$

$$p = 0.82-2j \quad (3)$$

$$h = 1.82-j \quad (4)$$

Rietveld analysis gives 74 wt.% jaffeite, 18 wt.% α-C_2SH and 8 wt.% portlandite, corresponding to molar proportions of 0.38, 0.25 and 0.28 mol, respectively. The molar proportions of jaffeite and α-C_2SH are consistent with the stoichiometric requirements of Eq. (2). From Eq. (3), the predicted amount of portlandite $p=0.07$ mol; from the Rietveld analysis we find a larger amount, 0.28 mol. Using Eq. (4) we calculate that the amount of water consumed in the reaction is $h=1.44$ mol. This corresponds to 0.10 BWOC, so that the original mix contains 0.30 BWOC excess water, expected to generate porosity in the final hydrated material.

We note that if the jaffeite is produced mainly by hydration of the alite phase and the α-C_2SH mainly by hydration of the belite phase, we would predict a jaffeite/α-C_2SH ratio of 1.03–1.13 (depending on whether Rietveld analysis or Bogue calculation from oxide analysis is used to estimate the alite and belite content of the cement), close to the observed j/c of 1.53. It is known [13,14] that phase pure C_3S produces only jaffeite at 150–200 °C, and that β-C_2S yields α-C_2SH below 220 °C [15]. However the long-term co-existence of these two phases (and portlandite) under hydrothermal conditions at 200 °C needs further investigation.

The rates of reaction can be observed by plotting the peak area versus time. Since there are uncertainties in the full-pattern Rietveld method for estimating the phase composition, we use the peak areas of single diagnostic peaks to compare the relative amount of phases present in samples. In addition, Rietveld analysis cannot be applied to energy dispersive data, and so the peak area method provides a consistent method applicable to both diffraction techniques presented here. For this reason peaks were selected that were present in both laboratory and energy

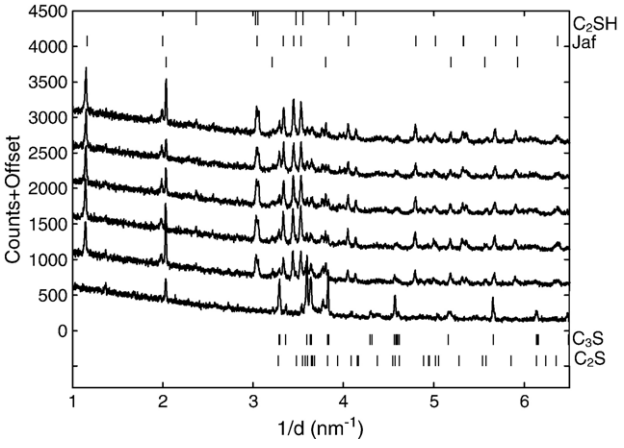

Fig. 2. Cement cured at 200 °C. Patterns plotted at 1, 2, 24, 48, 120 and 240 h curing time. ICDD peak positions for monoclinic C_3S, C_2S, portlandite (Por), jaffeite (Jaf) and α-C_2SH are shown.

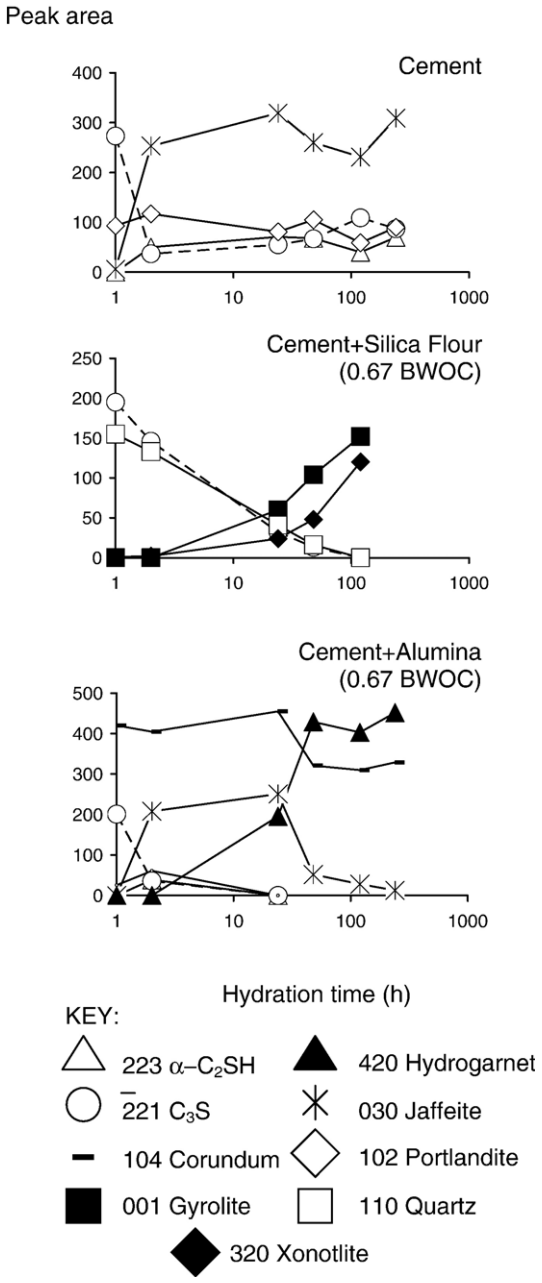

Fig. 3. Peak area versus curing time at 1, 2, 24, 48, 120 and 240 h for ex-situ samples. Note horizontal axis is plotted on a log scale for clarity at early stage hydration (<24 h).

dispersive data sets. Four diagnostic peaks were chosen to quantify alite, portlandite, jaffeite and α-C_2SH. These are the ($\bar{2}21$) alite peak at $1/d=3.29$ nm^{-1} ($d=3.04$ Å), the (102) portlandite peak at 5.17 nm^{-1} (1.93 Å), the (300) jaffeite peak at 3.45 nm^{-1} (2.90 Å) and the (223) peak of α-C_2SH at 4.14 nm^{-1} (2.42 Å). It should be noted that there is an overlap of the selected portlandite peak and the minor (2,2,10) peak of anhydrous alite, but this does not appear to have any great influence on the estimation of portlandite kinetics (Fig. 3).

Alite decreases rapidly within the first 2 h and may or may not be present together with belite after 24 h. It is difficult to say whether alite is consumed first and belite consumed later, as is commonly observed in cement at ambient temperatures, because of the complex peak overlap of these two clinker phases and the hydration products (Fig. 2). Jaffeite and α-C_2SH form during the first 2 h of hydration and thereafter the peak areas remain more or less constant, suggesting that the system stabilises relatively quickly (Fig. 3). Portlandite also forms during the first 2 h of hydration but appears to decrease slightly during the remaining hydration time. The formation and persistence of α-C_2SH are in keeping with previous observations of cement hydration at elevated temperatures [16] that crystallisation of C-S-H gel to α-C_2SH causes shrinkage and hence strength retrogression of such formulations. However, it should be noted that no gel phase is observed at any stage of hydration in our ex-situ experiments.

2.3. Dyckerhoff cement and silica at 200 °C

Silica flour was added to cement (0.67 BWOC) and heated for 1, 2, 24, 48 and 120 h (Fig. 4). Anhydrous calcium silicate phases (alite and belite) combine with silica to form an unidentified amorphous or very poorly crystalline C–S–H phase after 2 h, identified by a very broad hump in the background at 3.21 nm^{-1} (3.11 Å), which disappears after 5 days of hydration. Two crystalline hydrates, xonotlite C_6S_6H and gyrolite $C_8S_{12}H_{8-10.5}$, are observed to form by 48 h. Alite peaks are easily measurable at 24 h and a comparison between early time data from cement alone and from cement + silica shows that alite reacts more slowly in the presence of silica (Fig. 3); however, alite and belite disappear completely after 24 h. This suggests that the presence of silica initially retards hydration but then accelerates it after a certain time so that no anhydrous calcium silicates remain after 5 days.

The crystalline product phases are all calcium silicate hydrates, although the sample contains 7–8 wt.% of oxides other than C and S (Table 1). Gels in cements are usually referred to as C–S–H gels [17] as they commonly contain varying proportions of calcia, silica and water but they may

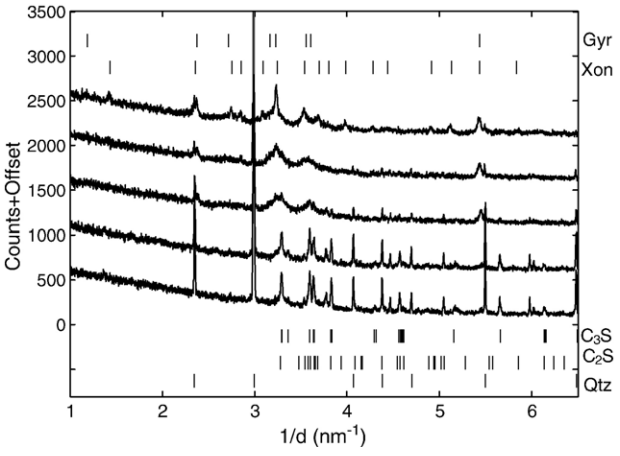

Fig. 4. Cement and silica flour (0.67 BWOC) cured at 200 °C. Patterns plotted at 1, 2, 24, 48 and 120 h curing time. ICDD peak positions for monoclinic C_3S, C_2S, quartz (Qtz), xonotlite (Xon) and gyrolite (Gyr) are illustrated.

easily incorporate other ions found in cement, e.g. Al, Fe. In addition to the gel phase, the gyrolite diffraction pattern is poor, with broad, low peaks. We can speculate that gyrolite with a notably complex crystal structure may have a high degree of lattice substitution. Lastly, the xonotlite may also contain ions other that Ca, Si or H, as has been found in naturally occurring samples [18].

For the longest curing times used, we can write the formal reaction

$$C_{2.82}S[\text{cement}] + 3.01S + hH \rightarrow xC_6S_6H + gC_8S_{12}H_{8-10.5} + qS \quad (5)$$

from which the following stoichiometric relations can be derived

$$x = 0.47-1.33g \quad (6)$$

$$q = 1.19-4g \quad (7)$$

$$8g + x \leq h \leq 10.5g + x \quad (8)$$

Rietveld analysis of the hydrated material gives 59 wt.% gyrolite, 36 wt.% xonotlite and 6 wt.% relict quartz, corresponding to molar amounts of 0.19, 0.21 and 0.43 mol, respectively. The molar proportions estimated from Rietveld analysis satisfy Eqs. (5)–(8) excellently.

The water content of gyrolite appears to be variable. Taylor [3] gives the formula of gyrolite as $C_8S_{12}H_8$, but more recent work by Merlino [19] suggests that the water content can vary, up to a maximum of $C_8S_{12}H_{10.5}$. The amount of water, h, required to form the hydrate phases and calculated from Eq. (8) lies in the range 1.75 to 2.23 mol. The corresponding range of water BWOS is 0.07 to 0.09 suggesting that somewhat less water is taken up by the system than when cement only is hydrated under these conditions. The excess of 0.31–0.33 water BWOS which is not chemically bound is expected to create porosity in the final hydroceramic product.

The effect of adding 0.67 silica BWOC has been to eliminate α-C_2SH which in turn should prevent strength retrogression. The presence of a gel phase is problematic. Little is known about its composition or how much is present. Furthermore, its presence during hydration may also cause some strength retrogression as is commonly considered to occur during the hydration of cement only at elevated temperatures [16]. However, the amount of silica used in our system is higher than that typically used downhole (0.35 BWOC). The mineralogy at lower silica additions might be expected to differ from that which we observe. However, what does appear to be of interest is the effect of silica addition on hydration rates. Initially this is reduced compared with cement alone, but then increases so that no anhydrous cement phases remain after 5 days hydration. The reasons for this are not yet clear.

2.4. Dyckerhoff cement and alumina at 200 °C

Alumina was added to cement (0.67 BWOC) and the mix cured for 1, 2, 24, 48, 120 and 240 h (Fig. 5). This is the only

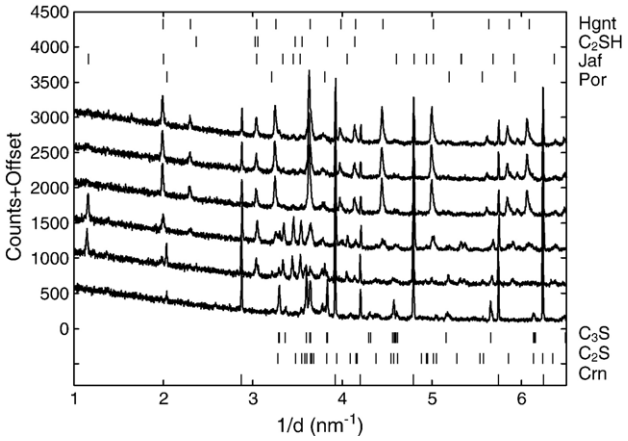

Fig. 5. Cement and alumina (0.67 BWOC) cured at 200 °C. Patterns plotted at 1, 2, 24, 48, 120 and 240 h curing time. ICDD patterns for monoclinic C_3S, C_2S, corundum (Crn), portlandite (Por), jaffeite (Jaf), α-C_2SH and hydrogarnet (Hgnt) are illustrated.

system to show intermediate phases. Initially the cement forms portlandite CH, α-C_2SH and jaffeite $C_6S_2H_3$. The rate of alite consumption (Fig. 3) is much the same as when alumina is absent. Clearly alumina does not retard the system in the way that added silica does during initial hydration.

The jaffeite and α-C_2SH are not stable and start to disappear within 24 h allowing the formation of hydrogarnet. It appears that the addition of alumina to the system destabilises both the jaffeite and α-C_2SH with respect to hydrogarnet. This is an important finding. It is known that many synthetic calcium silicate hydrates can take up a minor quantity of guest ions just as natural specimens do (see for example [18,19]) but at some point the excess must destabilise the calcium silicate hydrate structures in favour of hydrogarnet. Knowing this limit would be invaluable in predicting the stability of such hydroceramic CASH sealants in geothermal wells. These often contain brines which may destabilise the sealant if they come into contact with it before hydration is complete.

The calcium silicate hydrate phases, α-C_2SH and jaffeite, are almost completely consumed as the hydrogarnet forms, strongly suggesting that the hydrogarnet absorbs almost all the silica present in the original cement component. Hydrogarnet is identified in Fig. 5 using the hibschite $C_3AS_2H_2$ hydrogarnet pattern [ICCD 45–1447]. This pattern gives only an approximate indication of hydrogarnet peak locations in this system. Hydrogarnets form a solid solution series $C_3AS_{3-y}H_{2y}$, where y=1–3 roughly, and peak shifts are expected as a result of $SiO_4^{4-} \leftrightarrow 4OH^-$ substitution in the crystal structure [20,21]. The ratio S/H can be estimated from the observed d-spacings since the d-spacings in the solid-solution series vary linearly with y. For the hydrogarnet formed in our system, we find from the precise d-spacings of several prominent peaks that y=2.1 approximately, corresponding to a hydrogarnet composition $C_3AS_{0.9}H_{4.2}$.

The presence of hydrogarnet in hydrated cement or CASH pastes is not uncommon (e.g. [22–24]) but typically these hydrogarnets are essentially free of silica, with nominal

composition C_3AH_6 [25,26]. Hydrogarnets containing silica have been observed after less than 1 h in a synthesis reported by Klimesch and Ray [27,28]. However, their hydrogarnet converted to tobermorite after a few hours, an effect not observed in any samples we studied, even after curing for 10 days. So while Klimesch and Ray have created hydrogarnets in the CASH system previously, we report here the first direct in-situ observation of hydrogarnet synthesis from an oilwell cement precursor.

We can write the formal and simplified reaction

$$C_{2.82}S[\text{cement}] + 1.77A + hH \rightarrow kCa_3AlSi_{3-y}H_{2y} + jC_6S_2H_3 + aA \quad (9)$$

In Eq. (9) we neglect the small amount of alumina present in the cement (which is only about 5.2 wt.% of the total system alumina). The stoichiometry fixes the amounts of the products, and also the composition of the hydrogarnet if it is assumed that the small amount of jaffeite eventually disappears and j is zero. This gives us $k=0.94$ and $a=0.83$ for the predicted stoichiometric molar amounts of hydrogarnet and alumina (respectively). The value of y is predicted to be 1.94, close to the value of 2.1 estimated from the observed d-spacing. Rietveld analysis of the hydrated material gives 67 wt.% hydrogarnet, 30 wt.% corundum and 3 wt.% jaffeite, corresponding to molar amounts of 1.03, 1.83 and 0.04 mol, respectively. Rietveld analysis therefore finds too much relict alumina and too little hydrogarnet when compared with Eq. (9). If we include additional minor sources of alumina from the silicate and aluminoferrite phases of the cement the reaction scheme, the value of a is only increased slightly.

The amount of water required to balance Eq. (9) is 3.64 mol, equivalent to 0.15 BWOS. This is somewhat larger than for either cement only or with silica additions, but there is 0.25 BWOS excess water to generate porosity in the final product.

An important result of the analysis is that although unreacted alumina is present at the longest curing times, the hydrogarnet formed contains much more alumina than can be provided by the cement alone (0.94 and 0.096 mol, respectively). Therefore under these hydrothermal conditions the corundum alumina is certainly reactive; however, the residual alumina is not taken up by the hydrogarnet to form a more silica-poor hydrogarnet composition ($2.1<y<3$). Once all the silica is incorporated, the consumption of the remaining corundum ceases or at least becomes much slower.

3. In-situ experiments

3.1. Experimental details of in-situ experiments

While XRD gives us an idea of the major components of hydroceramics present after different curing times, we cannot be sure whether intermediate minor phases are present. In addition the presence of post-curing artefacts (e.g. calcite, scawtite) can clutter the data and make phase identification of trace phases difficult. The early time hydration behaviour (say <1 h) is especially difficult to investigate by ex-situ laboratory XRD. Therefore we have used in-situ energy dispersive diffraction (EDD) at the UK synchrotron radiation source SRS, Daresbury Laboratory, to complement our ex-situ studies.

The ex-situ compositions were repeated with EDD (Table 2). In addition the cement only sample was repeated at 250 °C to determine how increased temperature influences kinetics and phase assemblages. Each sample was mixed off-line and then loaded into a cylindrical cell (o.d. 12 mm, i.d. 10 mm, capacity 3 mL) designed by Lupo [29,30]. The cell is machined from 301 stainless steel and is fitted with a disposable PTFE liner. The cell has a stainless steel cap and is pressure-sealed by the flange of the liner. The cell has been designed to withstand an internal water vapour pressure of about 100 bar, and in systems containing free water provides a well-defined hydrothermal environment on the saturated vapour pressure curve of water. The sample is then placed in a purpose built oven [29,30]. A type-K thermocouple inserted into a well in the lid assembly provides temperature control. The sample is rotated at 1 s^{-1} to ensure good sample averaging. The oven and controller provide programmed temperature ramp and hold conditions. For our samples ramp times were 30 min; samples were then held at the target temperature for 10 h. The time delay between the start of hydration (initial mixing) and start of data acquisition is about 15 min, and each pattern was collected for 5 min. Water loss during hydration was at most 4% of the original sample weight and often much less.

Energy dispersive diffraction (EDD) experiments were carried out using white beam X-rays in the energy range 20–80 keV. The incident X-ray beam is shaped by a circular pinhole to 1.0 mm diameter, and diffracted X-rays then reach the detector at fixed (but adjustable) angles via flat plate collimators. The instrument acquires powder diffraction patterns from a well defined lozenge-shaped volume within the bulk sample [31]. A unique three-element detector in which diffracted X-rays are collected simultaneously at three different fixed diffraction angles is used to increase the range of accessible d-spacings [31]. The diffraction pattern from each detector has 4000 energy channels, the channel width being about 0.03 keV. Normally for cement based materials [23,32], we would utilize the bottom (low-angle) detector (highest d-spacings) but the steel cell used in the work we report here absorbs the lower energy wavelengths strongly and diffraction patterns from the hydrating sample are of poor quality with few identifiable peaks (Fig. 6). Data from the middle detector are found to be the most informative. The middle pattern is cleaner, with better signal:noise than both the top and bottom patterns. The energy-dispersive Bragg equation is $Ed\sin\theta = 0.61993$ keV nm. Thus there is a linear relationship between peak energy and reciprocal d-spacing, and it is convenient to re-scale the ordinate axis so as to display diffracted intensity against $1/d$. For these materials hydrated in a steel cell, we generally achieve a workable $1/d$ range of 2.5 to 6.5 nm^{-1} with the middle detector.

The width of the diffraction peaks of well crystallised components is typically <0.03 nm^{-1} (full-width half-maximum) in $1/d$ reciprocal space. The peaks are usually well represented by Gaussian lineshapes and overlapping peaks can often be

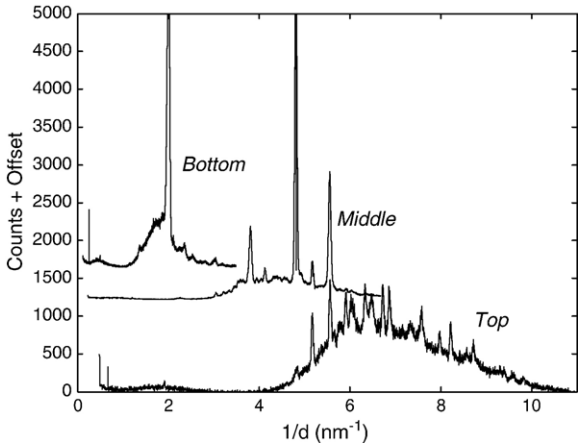

Fig. 6. Pattern 84 (7 h) of cement illustrating the variation in quality of data obtained from each detector when using the steel cell. For clarity the patterns have been offset vertically. Detector 2θ angles: bottom 1.999°, middle 4.902°, top 7.784°.

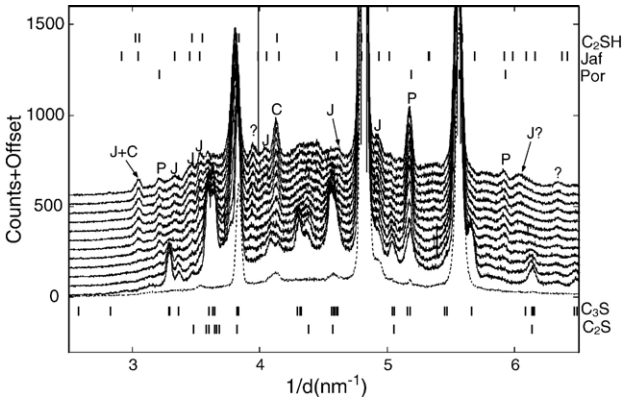

Fig. 8. Cement cured at 200 °C. Patterns plotted at 20, 70, 120, 170, 220, 270, 320, 370, 420, 470, 520 and 570 min. The dotted pattern is the empty steel cell and PTFE liner. ICDD patterns for C_3S, C_2S, jaffeite (Jaf), α-C_2SH and portlandite (Por) are illustrated and the individual peaks of hydration phases, jaffeite (J), α-C_2SH (C) and portlandite (P) are labelled.

deconvolved successfully. The error in the position ($1/d$) of a peak fitted to a Gaussian lineshape function is about 0.001 nm^{-1}. Therefore, even for broad peaks, relative peak positions and shifts (for example within a single hydration run) can be determined accurately. Absolute calibration of d-spacings is made with suitable mineral standards, usually gypsum. A correction for the slow decay in synchrotron X-ray intensity during an experiment is made by normalising detector counts within a single experimental shift to constant synchrotron beam current. In addition the intensities have also been corrected for day-to-day variations in the beam.

3.2. Dyckerhoff cement at 200 °C

The laboratory XRD and synchrotron EDD data are compared in Fig. 7. We see that although signal:noise ratio is better in the EDD data the peak resolution is poor. The steel cell absorbs much of the beam flux and in addition diffracts, adding several intense peaks to the pattern. Hence we are unlikely to find trace or minor intermediate or product phases. It is also noted that the peaks are much broader and hence overlapping peaks are difficult to distinguish. This aside, sufficient peaks are available to enable us to identify the main product phases, the timing of mineral transformations and to estimate the rates of reaction.

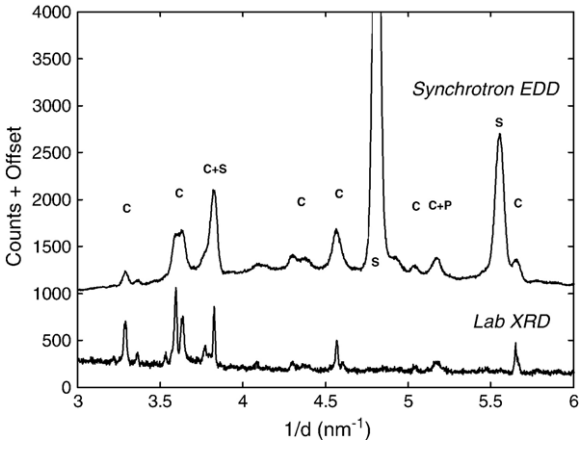

Fig. 7. Comparison of laboratory XRD and synchrotron EDD data for cement at 1 h hydration (S=steel; C=cement; P=portlandite).

At the outset, alite and belite dominate the pattern (Fig. 8). As in the ex-situ experiments three secondary phases are then identified: portlandite, α-C_2SH and jaffeite. This is consistent with the laboratory XRD patterns (Fig. 2) in which these three phases are observed after 2 h curing time and appear to grow during the course of the experiment. The same peaks identified as suitable for curve fitting in the laboratory XRD data are also used in the analysis of EDD data (Fig. 9), with the exception of jaffeite. Jaffeite is not observed as clearly (or not formed to the same extent) in the in-situ experiments as in the ex-situ, and although the peaks can be identified in EDD data they are inferior and unsuitable for peak fitting.

As many more patterns are collected in the EDD experiments, we have finer time-slicing and reaction curves are better defined. We can therefore estimate approximate reaction rates by normalising the rate of increase of peak area (dA/dt) by the peak area A_n at some suitable time [23]. For anhydrous phases this is taken as being that of the first pattern, $n=1$. Hence the reaction rate constant $k=1/A_n \cdot dA/dt$, $n=1$. (The sign convention here differs from that which we used in a previous publication [23], in order to have positive values of k for product phases and negative values for phases which are being consumed.) The alite peak at 3.29 nm^{-1} yields a reaction rate constant k of −0.3 h^{-1}. For product phases, portlandite and α-C_2SH, peak areas are normalised by the area of a fully developed late peak: n is taken as 114 (the area of the peak of interest in pattern 114). The changes in portlandite and α-C_2SH peak intensity yield formation rate constants of 0.04 and 0.09 h^{-1} (respectively). It should be noted that the portlandite formation rate constant was estimated from late time data; the initial rate of formation must have been greater.

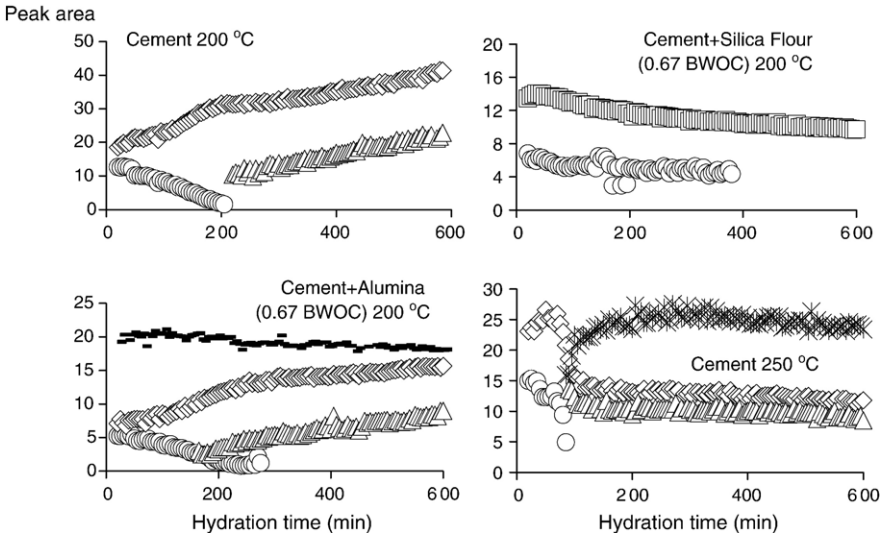

Fig. 9. Peak areas versus hydration time for each in-situ sample. Key as for Fig. 3.

However, we cannot quantify an earlier rate of reaction with confidence because of overlap with the minor (2,2,10) alite peak at $1/d = 5.18$ nm^{-1} ($d = 1.93$ Å).

The rates of reaction are not easy to compare with previous published work because the starting materials differ somewhat. Portlandite is frequently seen after the initial hydration of cement both at ambient and higher temperature but the synthesis of α-C_2SH and jaffeite is less well documented. Where it has been synthesised, either in-situ or ex-situ, the starting materials are commonly different. The presence of α-C_2SH has been noted as deleterious to sealant formation earlier in this paper (Section 2.2); however, the presence of jaffeite, and its possible effects, are not commonly mentioned. Jaffeite has been little studied in-situ and unfortunately previously published studies have used a variety of starting materials. Wang and Tomita [33] using lime and quartz as reagents observed that jaffeite forms in less than 3 h at 300 °C but not at all even after 12 h at 175 °C. Taylor [3], Hu *et al.* [34] and Barnes *et al.* [13] use different starting compositions (lime and silica, β-C_2S and silica and C_3S, respectively), yet all observe the formation of jaffeite below 300 °C. Indeed Taylor (Fig. 1) and Barnes *et al.* find jaffeite below 200 °C, the starting composition used by Barnes *et al.* being perhaps the closest model for a real cement and hence the closest with which to compare our system. Jaffeite is first detected by Barnes *et al.* at 130 min at 150 °C, while we observe the appearance of well crystallized jaffeite within 2 h ex-situ and in a poorly crystalline form in-situ within 5 h at the higher temperature of 200 °C. Why poorly crystalline jaffeite should form in in-situ experiments is not clear.

3.3. Dyckerhoff cement and silica at 200 °C

When silica flour (0.67 BWOC) is added to the cement, we observe that little happens in the first 10 h of curing (Fig. 10). Both the calcium silicate phases and the quartz persist throughout the experiment and the only secondary phase appears to belong to the amorphous or poorly crystalline phase noted earlier in Section 2.3 (compare Figs. 4 and 10). No other new peaks are noted hence no crystalline secondary phases form within the time frame of the in-situ experiments and this corroborates the ex-situ data.

The depletion of alite (Fig. 9) occurs with a rate of reaction of -0.04 h^{-1}, and so is initially consumed significantly more slowly than it is in a cement with no added silica. This is also observed in the XRD data (Fig. 4) where poorly crystalline hydrate is observed after 2 h but does not appear to form identifiable peaks until after 24 h. A slower rate of hydration suggests that the system is being retarded in the early stages (<24 h) by the addition of silica. Previous data [35] indicate that the addition of silica reduces thickening times and accelerates setting. The formation of the amorphous or poorly crystalline gel may also impede hydration by coating the anhydrous phases and initially slowing down further hydration. The early gel may

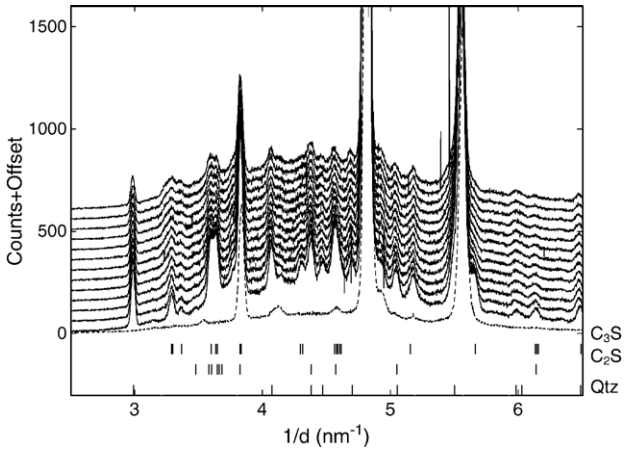

Fig. 10. Cement and silica flour (0.67 BWOC) cured at 200 °C. Patterns plotted at 20, 70, 120, 170, 220, 270, 320, 370, 420, 470, 520, 570 and 620 min. The dotted pattern is the empty steel cell and PTFE liner. ICDD patterns for C_3S, C_2S and quartz (Qtz) are illustrated.

also increase the viscosity of the slurry hence reducing thickening times. What triggers hydration to continue and crystalline products to form is not known. This is an important question in relation to cement hydration at any temperature when an early gel appears to halt hydration temporarily (that is, to create a dormant period).

3.4. Dyckerhoff cement and alumina at 200 °C

With the addition of alumina (0.67 BWOC) we see the familiar secondary phases of portlandite, α-C_2SH and jaffeite (Fig. 11), as observed for cement with no additions. This is the intermediate phase assemblage observed in ex-situ experiments prior to hydrogarnet formation (Fig. 5). No hydrogarnet is observed in the in-situ experiments, which last up to 10 h. This is consistent with in the ex-situ experiments which show the first appearance of hydrogarnet at the later time of 24 h (Figs. 3 and 5). The secondary phase development here is similar to that which we observe in the cement-only system, alite having a reaction rate constant of about -0.2 h^{-1}, although peak intensity is reduced (compare Fig. 9). Similarly the amounts of secondary phases produced are reduced too, but reaction constants are comparable ($k=0.03$ h^{-1} for the formation of portlandite, and $k=0.09$ h^{-1} for the formation of α-C_2SH). Jaffeite formation is less conspicuous than in the ex-situ experiments, just as was observed for the cement only system. As alumina is still abundant at the end of the experiment it seems that it is less reactive than the cement although it does decrease slightly during the course of the experiment (Figs. 9 and 11). The cement itself reacts at much the same rate as it does in the absence of the alumina.

3.5. Dyckerhoff Cement at 250 °C

At 250 °C the secondary phase assemblage remains much the same as at 200 °C (Fig. 12) but there are two striking differences.

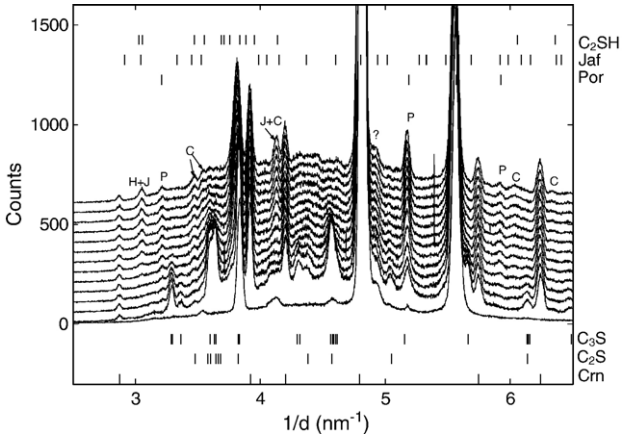

Fig. 11. Cement and alumina (0.67 BWOC) cured at 200 °C. Patterns plotted at 20, 70, 120, 170, 220, 270, 320, 370, 420, 470, 520, 570 and 620 min. The dotted pattern is the empty steel cell and PTFE liner. ICDD patterns for C_3S, C_2S, jaffeite (Jaf), α-C_2SH, portlandite (Por) and corundum (Crn) are illustrated and the individual peaks of hydration phases jaffeite (J), α-C_2SH (C) and portlandite (P) are labelled.

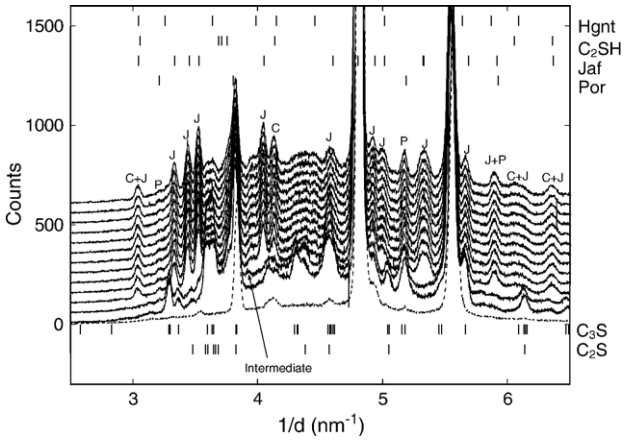

Fig. 12. Cement cured at 250 °C. Patterns plotted at 20, 70, 120, 170, 220, 270, 320, 370, 420, 470, 520, 570 and 620 min. The dotted pattern is the empty steel cell and PTFE liner. ICDD patterns for C_3S, C_2S, jaffeite (Jaf), α-C_2SH and portlandite (Por) are illustrated and the individual peaks of hydration phases jaffeite (J), α-C_2SH (C) and portlandite (P) are labelled.

First the anhydrous calcium silicate phases are consumed much faster ($k=0.4$ h^{-1} for alite depletion); and the proportions of secondary phases are clearly increased including jaffeite, previously forming only small insignificant peaks but now forming large clearly identifiable peaks. Rate constants for portlandite and α-C_2SH formation yield unusual values of -0.02 and -0.03 h^{-1} (respectively) suggesting they are being slowly consumed (Fig. 9). As the only other secondary phase observed at this stage is jaffeite, it must be assumed that portlandite and α-C_2SH are being consumed to form jaffeite (although jaffeite peak areas do not increase markedly after 2 h).

4. Comment on the structural succession

Our aim is to optimize cementing systems for severe hydrothermal service conditions. Work in progress extends the temperature range to 350 °C and above. While the picture is far from complete, we can make some comments on structural aspects of the hydrated minerals formed in the experiments we report here.

First, we note a tendency to form rather simple product assemblages. In the case of cement alone, we form jaffeite (silicate dimers) and α-C_2SH (isolated silicate units) at 200 °C, roughly in proportion to the alite/belite proportions of the cement, with only a small amount of portlandite. There is an indication that at 250 °C the portlandite may be absorbed to form further jaffeite, which is known to be stable up to at least 400 °C. The scope for further condensation of silicate is severely limited by the constraint of cation/anion charge balance.

In the case of cement + silica, we observe a product phase assemblage which contains only xonotlite (double silicate chains) and gyrolite (silicate sheet layer structure). The much greater condensation of silicate units is made possible by the lower C/S ratio, and we are able to produce robust products with thermal stability extending to 500 °C and above. Furthermore we may expect the presence of silicate sheets and chains to bring mechanical benefits to the bulk material.

In the case of cement+alumina, the product is a single hydrogarnet phase in the katoite-hibschite series. The substitution of silica units (with charge balancing by loss of OH^-) in the hydrogarnet allows the cement silica to be absorbed.

Above 200 °C, the water in all these product phases is present as hydroxide; simple water of crystallization is not found. The amount of mix water which is incorporated within the solid is therefore smaller than in ambient temperature cement hydration, and this no doubt leads to substantial porosity in the bulk hydrated material, unless compaction can be achieved. However, the amount of OH^- incorporated in the hydrogarnets is greater than in the xonotlite and gyrolite silicate hydrates, which in turn is greater than for jaffeite and α-C_2SH.

5. Conclusions

Ex-situ and in-situ experiments each have their advantages as we demonstrate.

Laboratory hydrothermal syntheses can be performed for long periods of time; ex-situ XRD analysis gives higher quality peak resolution; but gives poorer time resolution because of uncertainty in quenching time. In-situ hydrothermal experiments can usually only be of limited duration (say <12 h) because of limits on beamtime access. At and above 200 °C they give poorer peak resolution because of high X-ray attenuation and diffraction by the steel cell; but give better time resolution.

Our ex-situ data show that an oilwell-type portland cement hydrates to jaffeite, α-C_2SH and portlandite at both 200 and 250 °C in the presence of excess water at its saturated vapour pressure. This is in line with the findings of previous authors whereby the presence of α-C_2SH is considered deleterious to sealant strength. At 200 °C the majority of the system reaches equilibrium within a relatively short period of time (<24 h) regarding secondary hydrates; however, anhydrous calcium silicate phases appear to persist until even after 10 days. Hence not only is its strength compromised but a lengthened setting process could cause problems when setting a real well environment. However, this setting time could be reduced at higher temperatures. Rietveld refinements of the final hydrated product are in good agreement with stoichiometry of the system; however, portlandite tends to be overestimated using this method of quantification.

When silica is added to the system early hydration (<24 h) is retarded and only poorly crystalline precursor phases are observed within 12 h. Crystalline hydrates are not observed until after 48 h, when the rate of consumption of the primary anhydrous calcium silicates increases. No primary clinker phases can be detected after 5 days hydration. Rietveld refinement of the final hydration product is in good agreement with the stoichiometry of the system. As these sealants are commonly used in high temperature wells the possibility of early stage retardation needs to be considered. If confirmed, early setting times would be extended by the addition of silica and such formulations would be more vulnerable to attack by geothermal brines during hydration.

When alumina is added to the cement, we observe first intermediate jaffeite and α-C_2SH, which are later absorbed into hydrogarnet. The presence of alumina does not appear to much alter reaction rates, neither accelerating nor retarding the system. Some relict corundum is observed after 10 d curing, so that it is possible that complete equilibrium has not been attained or that a saturation point is reached for the hydrogarnet with respect to alumina. Rietveld refinement of the final hydration product assemblage is in good agreement with stoichiometry for hydrogarnet but appears to overestimate the amount of unreacted alumina.

Acknowledgements

We thank the UK EPSRC for financial support, CCLRC for synchrotron beamtime, Alfie Neild and David Taylor (Daresbury Laboratory) for technical support, and Simon Jacques and Fabio Lupo (Industrial Materials Group, Birkbeck University of London and University College London) for the use of a purpose-built oven on the synchrotron beamline. We acknowledge the use of the EPSRC's Chemical Database Service at Daresbury.

References

[1] G. Carter, D.K. Smith, Properties of cementing compositions at elevated temperatures and pressure, Trans. Metall. Soc. AIME 213 (1958) 20–27.
[2] E. Nelson, Well Cementing, Schlumberger Educational Services, Sugar Land, Texas, 1990.
[3] H.F.W. Taylor, The calcium silicate hydrates, in: H.F.W. Taylor (Ed.), The Chemistry of Cements, Academic Press, London, 1964, pp. 168–232.
[4] V. Barlet-Gouédard, S. Danican, E. Nelson, C. Cambus, Cement compositions for high temperature applications, PCT Patent Application WO 03/068708, 21 August 2003.
[5] V. Barlet-Gouédard, B. Goffé, Cementing compositions and application of these compositions to cementing oil wells or the like, PCT Patent Application WO 01/70646, 27 September 2001.
[6] V. Barlet-Gouédard, B. Vidick, A non-conventional way of developing cement slurry for geothermal wells, Geotherm. Res. Counc. Trans. 25 (2001) 85–91.
[7] N. Meller, C. Hall, Hydroceramic sealants for geothermal wells, in: M. Pecchio, F.R.D. Andrade, L.Z.D. D'Agostino, H. Kahn, L.M. Sant'Agostigno, M.M.M.L. Tassinari (Eds.), International Congress on Applied Mineralogy, Internation Council for Applied Mineralogy do Brasil, 2004, pp. 281–284.
[8] N. Meller, C. Hall, J. Phipps, A new phase diagram for the $CaO–Al_2O_3–SiO_2–H_2O$ hydroceramic system at 200 °C, Mater. Res. Bull. 40 (2005) 715–723.
[9] C. Hall, K.L. Scrivener, Oilwell cement clinkers-X-ray microanalysis and phase composition, Adv. Cem. Based Mater. 7 (1998) 28–38.
[10] E. Nelson, L.H. Eilers, Cementing steamflood and fireflood wells-slurry design, J. Can. Pet. Technol. 25 (5) (1985) 58–63.
[11] K.L. Scrivener, T. Fullmann, E. Gallucci, G. Walenta, E. Bermejo, Quantitative study of Portland cement hydration by X-ray diffraction/Rietveld analysis and independent methods, Cem. Concr. Res. 34 (2004) 1541–1547.
[12] D.A. Fletcher, R.F. McMeeking, D. Parkin, The United Kingdom chemical database service, J. Chem. Inf. Model. 36 (1996) 746–749.
[13] P. Barnes, S.L. Colston, A.C. Jupe, S.D.M. Jacques, M. Attfield, R. Pisula, S. Morgan, C. Hall, P. Livesey, S. Lunt, The use of synchrotron sources in the study of cement materials, in: J. Bensted, P. Barnes (Eds.), Structure and Performance of Cements, Spon Press, London, 2002.
[14] N. Meller, C. Hall, K. Kyritsis, G. Giriat, H. J. Jakobsen, J. Skibsted, Incorporation of aluminium guest ions in nominally alumina-free calcium

silicate hydrates: effects on crystal structure and thermal stability, in Proceedings of the 12th International Congress on the Chemistry of Cement, Montreal, July 2007.
[15] K. Yanagisawa, X. Hu, A. Onda, K. Kajiyoshi, Hydration of β-dicalcium silicate at high temperatures under hydrothermal conditions, Cem. Concr. Res. 36 (2006) 810–816.
[16] E. Nelson, Thermal cements, in: E. Nelson (Ed.), Well Cementing, Schlumberger Educational Services, Sugar Land, Texas, 1990.
[17] H.F.W. Taylor, Cement Chemistry, Thomas Telford Publishing, London, 1997.
[18] J.J. Esteban, J. Cuevas, J.M. Tubia, Xonotlite in rodingite assemblages from the Ronda Peridotites, Betic Cordilleras, southern Spain, Can. Mineral. 41 (2003) 161–170.
[19] S. Merlino, Gyrolite: its crystal structure and crystal chemistry, Mineral. Mag. 52 (1988) 377–387.
[20] R. Siauciunas, A. Baltusnikas, Influence of SiO_2 modification on hydrogarnets formation during hydrothermal synthesis, Cem. Concr. Res. 33 (2003) 1789–1793.
[21] J.M. Rivas Mercury, X. Turrillas, A.H. de Aza, P. Pena, Calcium aluminates hydration in presence of amorphous SiO_2 at temperatures below 90 °C, J. Solid State Chem. 179 (2006) 2988–2997.
[22] A.C. Jupe, A.P. Wilkinson, K. Luke, G.P. Funkhouser, Class H oil well cement hydration at elevated temperatures in the presence of retarding agents: an in situ high energy X-ray diffraction study, Ind. Chem. Eng. Res. 44 (2005) 5579–5584.
[23] N. Meller, C. Hall, A.C. Jupe, S.L. Colston, S. Jacques, P. Barnes, J. Phipps, Time resolved studies of the hydration of brownmillerite with and without gypsum: a synchrotron diffraction study at ambient and elevated temperature, J. Mater. Chem. 14 (3) (2004) 428–435.
[24] S. Shaw, C.M.B. Henderson, S.M. Clark, Hydrothermal synthesis of cement phases: an in situ synchrotron energy dispersive diffraction study of reaction kinetics and mechanisms, High Press. Res. 20 (2001) 311–3204.
[25] A.C. Jupe, X. Turrillas, P. Barnes, S.L. Colston, C. Hall, D. Häusermann, M. Hanfland, Fast in situ X-ray diffraction studies of chemical reaction: a synchrotron view of the hydration of tricalcium aluminate, Phys. Rev. 53 (1996) 14697–14700.
[26] P. Meredith, A.M. Donald, N. Meller, C. Hall, Tricalcium aluminate hydration: microstructural observation by in situ electron microscopy, J. Mater. Sci. 39 (3) (2004) 997–1005.
[27] D.S. Klimesch, A.S. Ray, Effect of quartz content on the nature of Al-substituted 11Å tobermorite in hydrothermally treated $CaO–Al_2O_3–SiO_2–H_2O$ systems, Adv. Cem. Res. 11 (4) (1999) 179–187.
[28] D.S. Klimesch, A.S. Ray, DTA-TGA evaluations of the $CaO–Al_2O_3–SiO_2–H_2O$ system treated hydrothermally, Thermochim. Acta 334 (1999) 115–122.
[29] F. Lupo, J.K. Cockroft, P. Barnes, P. Stukas, M. Vickers, C. Norman, H. Bradshaw, Hydrothermal crystallisation of doped zirconia: an in-situ X-ray diffraction study, Phys. Chem. Chem. Phys. 6 (8) (2004) 1837–1841.
[30] F. Lupo, Studies on crystallisation of zirconia under hydrothermal conditions, PhD Thesis, University of London, 2002.
[31] P. Barnes, A.C. Jupe, S.L. Colston, S. Jacques, A. Grant, T. Rathbone, F.M. Miller, S.M. Clark, R.J. Cernik, A new three-angle energy-dispersive diffractometer, Nucl. Instrum. Methods Phys. Res., B Beam Interact. Mater. Atoms 134 (1998) 310–313.
[32] S.L. Colston, P. Barnes, A.C. Jupe, S. Jacques, C. Hall, P. Livesey, J. Dransfield, N. Meller, An in situ synchrotron energy-dispersive diffraction study of the hydration of oilwell cement systems under high temperature/autoclave conditions up to 130 °C, Cem. Concr. Res. 35 (12) (2005) 2223–2232.
[33] J. Wang, A. Tomita, Hydrothermal reaction of $Ca(OH)_2$ with quartz in connection with coal demineralisation, Ind. Eng. Chem. Res. 36 (1997) 1464–1469.
[34] X. Hu, K. Yanagisawa, A. Onda, K. Kajiyoshi, Stability and phase relations of dicalcium silicate hydrates under hydrothermal conditions, J. Ceram. Soc. Jpn. 114 (2) (2006) 174–179.
[35] J. Bensted, Thickening behaviour of oilwell cement slurries with silica flour and silica sand additions, Chem. Ind. 18 (1992) 702–704.